Vol. 5 No. 4
Autumn 1994

ROTATIONAL ASSIGNMENT OF NEW BANDS IN THE NO_2 EXCITATION SPECTRUM IN THE SPECTRAL RANGE OF 15600 cm^{-1} TO 15633 cm^{-1}

E. Mehdizadeh*[1] and W. Demtröder[2]

[1] *Department of Physics, Shahid Bahonar University of Kerman, Kerman, 76175, Islamic Republic of Iran*
[2] *Fachbereich Physik, Universität Kaiserslautern, 6750 Kaiserslautern, Germany*

Abstract

Sub-Doppler excitation spectroscopy in a collimated cold supersonic beam of 5% NO_2 seeded in argon has been performed with a spectral resolution down to 10 MHz for four vibronic bands within the perturbed $^2B^2 \leftarrow X^2A$ system of NO_2. The rotational temperature of about 15 K achieved by adiabatic cooling allows the separation of closely lying vibronic bands which overlap in absorption spectra taken at room temperature and which therefore could not be identified from the broad band excitation measurements.

Introduction

During the last few years, the visible range of the NO_2 absorption spectrum has been the subject of intense investigations, using various experimental methods with different degrees of spectral resolution [1-5]. This spectrum represents a spectroscopic problem of outstanding complexity which shows many anomalies. The number of vibronic band origins exceeds by far that expected from the calculated vibrational level density in the $^2B_2$ state [6]. The intensities of the vibrational bands generally do not follow the Franck-Condon pattern of unperturbed transitions [7] and the Landé-factors obtained from optical-rf double-resonance measurements show a more or less irregular behavior for the different rotational levels in the upper vibronic state which is correlated with the measured hfs-splitting of these levels [8].

Several theoretical investigations [9-13] have contributed to a better understanding of the various coupling mechanisms between different electronic states of NO_2. The results of these experimental and theoretical efforts may be summarized as follows: The causes of the observed spectral congestions are manifold. Firstly, a strong nonlinear vibronic coupling between vibronic levels in the excited $^2B_2$ state with densely spaced high lying levels in the electronic ground state X^2A_1 due to a conical intersection of the two potential surfaces [12] leads to a chaotic energy level distribution [3-5]. Furthermore, the spin-rotation splitting, due to the spin s=1/2 of the unpaired electron and the hyperfine-structure, mainly caused by Fermi-interaction of this electron with the nuclear spin I=1 of the ^{14}N nucleus both lead to a splitting of the rotational levels into fine-and hyperfine components and therefore increase the line density of the already complex asymmetric rotor spectrum.

The strong vibronic interaction causes a mixing between radiative and "dark" levels, which results in large variations of the radiative lifetimes with excitation energy [14]. Even within a vibronic band, the lifetimes vary with the rotational quantum number, which can be traced to spin-orbit coupling and Coriolis-coupling [8, 15, 16]. The vibronic coupling also affects the rotational constants of rotational levels within a vibronic state.

Keywords: Laser spectroscopy; Supersonic molecular beams; Visible NO_2 spectrum

Spectroscopy with sub-Doppler resolution, which allows one to resolve not only the rotational structure, but also the fine-and hyperfine structure is therefore demanded in order to investigate all these anomalies in detail.

The present paper reports on such more detailed investigations of four vibronic bands, where the line positions have been determined with an accuracy of 10^{-3} cm^{-1}. In order to reduce the number of absorbing rotational levels and to avoid spectral overlaps of different bands, the NO_2 molecules are cooled by adiabatic expansion of an argon-NO_2 mixture (5% NO_2, 95% argon, total pressure 1 bar) into the vacuum. Thus, a rotational temperature $T_{rot} \approx 15$ K could be achieved, which compressed the rotational population into the lowest rotational levels with a maximum population at N" = 3.

Experimental Section

The experimental arrangement is shown in Figure 1. The beam of a stabilized tunable single-mode cw dye laser is crossed perpendicularly with a collimated supersonic beam of 5% NO_2 in argon. Depending on the chosen collimation ratio (typical values were 1:100) linewidths down to 10 MHz in the sub-Doppler excitation spectra could be achieved. The supersonic beam emerges from a reservoir (at a total pressure of up to 1 bar) through a nozzle of 50 μm diameter. The beam collimation is performed by a skimmer of 1 mm diameter at a distance of 50 mm from the nozzle, in a wall which separates the excitation region from the first chamber and which allows differential pumping. A diffusion pump (5000 1/s) backed by a roots pump maintains a background pressure of $\simeq 1 \times 10^{-4}$ bar between nozzle and skimmer. However, the background pressure in the differentially pumped excitation chamber (extra pump with 2000 1/s) is below 1×10^{-6} mbar with the beam off and rises to 4×10^{-6} mbar with the beam on. Because of the long radiative lifetimes of the excited NO_2 states (30-150 μs) [15, 16] the excited molecules with a mean velocity of 600 m/s may travel several centimeters from the point of excitation before they emit a fluorescence photon. It is, therefore, more efficient to collect the fluorescence in the direction of the molecular beam rather than perpendicular to it. The fluorescence is imaged by a lens L1 (f=90 mm) and a spatial filter consisting of two lenses L2 and L3 (f_2 = 140 mm, f_3 = 50 mm) with a pinhole in the focal plane of L2 onto the cathode of the photomultiplier. This arrangement has two advantages:

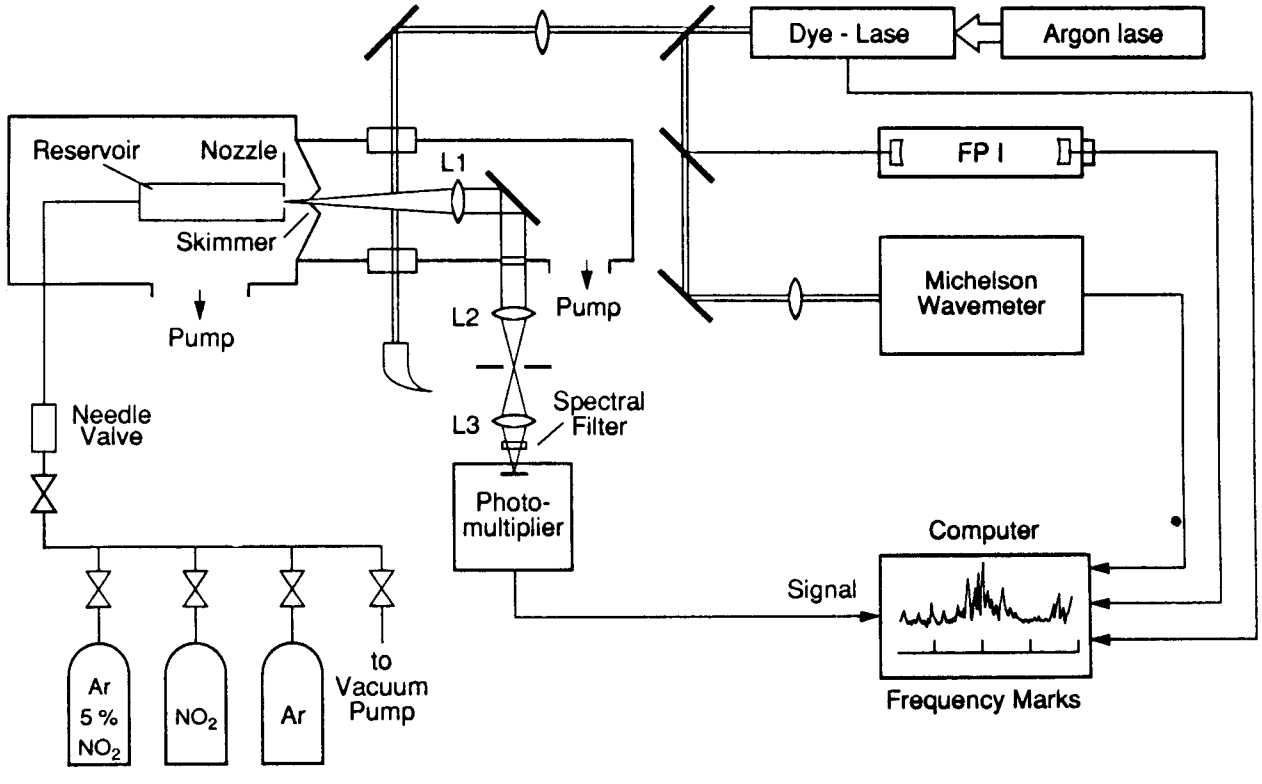

Figure 1. Schematic diagram of the experimental setup

Firstly, this spatial filter reduces the background signal caused by scattered laser light considerably. The residual scattered light can be completely suppressed by a spectral cut-off filter. Secondly, it allows a constant detection efficiency for the fluorescence emitted at different points z_e along the molecular beam axis, if only L1 with focal length f at a distance z_0 from the excitation point and two apertures with diameter D at the lens L1 and with diameter d in front of the multiplier cathode are used. It can be readily shown [16] that the fluorescence emitted from all points z_e within the interval $f \leq z_0 - z_e \leq f \cdot D/d$ is collected with the same efficiency, i.e. within the same solid angle.

This arrangement allows equal detection of all emitting molecules and the excitation spectrum obtained in this way therefore reflects the true absorption spectrum as long as saturation effects can be neglected. On the other hand, a perpendicular detection arrangement favors the short-lived emitting levels. If the excitation spectrum is simultaneously recorded by the two arrangements, a comparison between the intensity of the two spectra allows distinction between unperturbed levels of the $^2B_2$-state (with a short lifetime) and strongly perturbed levels (with a much longer lifetime) [15].

While the excitation spectrum is recorded, frequency marks separated by 63 MHz are generated by sending a small fraction of the laser beam through a 120 cm long confocal Fabry-Perot interferometer, (FPI), which is vacuum-tight and compensated for temperature drifts. These marks are recorded simultaneously with the spectrum. For high accuracy spectroscopy they are essential because the scan of the dye laser is not strictly linear and deviations from a linear ramp up to 100 MHz have been observed. With the help of the FPI frequency marks, a computer program can correct these deviations and can calculate the correct line positions in the spectrum.

Absolute wavelength calibration is performed with a Michelson-type travelling wavemeter [17] which uses a He-Ne-laser, stabilized onto the hfs-component K in the rotational transition $B^3\Pi_{ou}$ (v'=8, J'=53) $\leftarrow X^3\Sigma_g$ (v" = 4, J" = 54) of the iodine isotope molecule $^{129}I_2$ with a vacuum wavelength λ_R ($^{129}I_2$, k) = 632.991269 nm as reference wavelength standard [18]. The accuracy of the absolute wavenumber measurements is better than $\pm 10^{-3}$ cm^{-1} ($\Delta\nu \leq 30$ MHz).

Results and Discussion

In the broadband excitation measurements reported by Persch *et al.* [3], the rotational structure was not resolved. The vibronic bands of the $^2B_2 \leftarrow X^2A_1$ system could be distinguished from those of the overlapping $^2B_1 \leftarrow X^2A_1$ system by a contour analysis. This analysis was based on the fact that the Q-lines are strong for the $^2B_1$ bands but weak for the $^2B_2$ - X^2A_1 system. The missing Q-lines cause a dip in the band intensity profile at the band origin between the P branch and the R branch. This dip was used to identify the band origin of the $^2B_2$-bands. However, this relatively simple shape recognition technique is not always safe. It fails for overlapping bands where the dip may be filled by rotational lines of the neighboring band. Therefore, high resolution measurements are necessary to separate such bands and to reach an unambiguous assignment.

A section of such a cold sub-Doppler spectrum is shown in Figure 2. The rotational temperature can be calculated from the intensity ratios I(P)/I(R) of P and R lines with the same upper level N', i.e. P(N" = N'+1) and R(N" = N'-1) in the subband with $K_a = 0$. Assuming a Boltzmann distribution among the rotational level population n"(J", $K_a'' = 0$) we obtain the relation

$$\frac{n_i}{n_k} = \frac{g_i}{g_k} e^{-(E_i - E_k)/kT_{rot}} \qquad (1)$$

for the level population densities n_i'', n_k'' with g = (2J + 1) and J = N ± 1/2. With the Hönl-London factors [19] the rotational temperature

$$T_{rot} = \frac{\Delta E}{k \cdot ln\left(\frac{a_1 I_R}{a_2 I_P}\right)} \qquad (2)$$

can be calculated from the measured intensities I_P, I_R of P-and R-lines [20]. ΔE is the energy separation between the P-and R-line with a common upper level N', k is the Boltzmann constant and the factors a_1, a_2 depend on the statistical weight factors g_1, g_k and on the Hönl-London factors.

The assignment of the rotational transitions is based on several criteria: First of all the ground state differences for lines terminating at the same upper level N''_{K_a,K_c} (s = ± 1/2), which are accurately known from infrared [21] and microwave [22] spectroscopy of NO_2, allow in most cases an unambiguous assignment. At an accuracy of 10^{-3} cm^{-1} of our measured positions, these ground state-differences should match the microwave data by at least 0.002 cm^{-1}. At the low rotational temperatures, the levels with $K_a = 0$ are much more populated than those with $K_a \geq 1$. The parallel transitions of the $^2B_2 \leftarrow X^2A_1$ system with $\Delta K_a = 0$ are therefore strongest for $K_a = 0$. Further

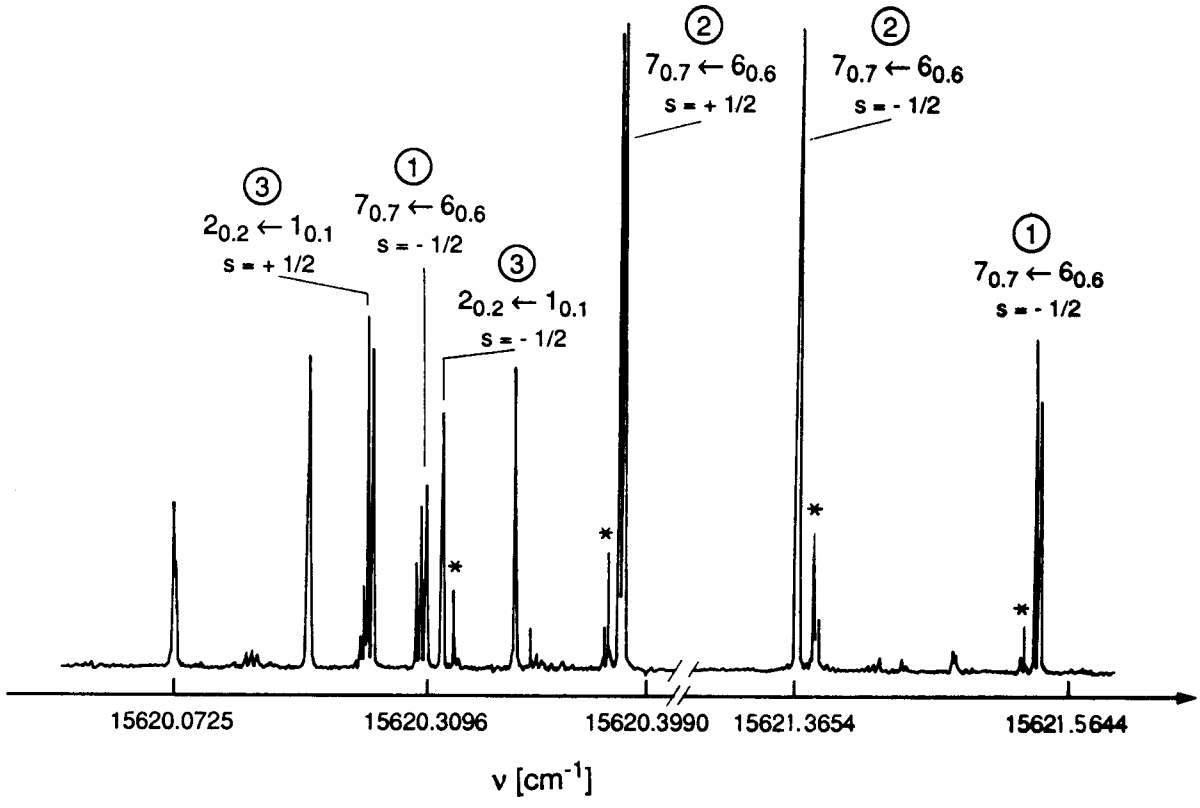

Figure 2. Section of the sub-Doppler spectrum of NO_2 around 15620 cm^{-1} illustrating the superposition of three vibronic bands. The numbers in circles give the band number in Table 1. The transitions with an asterix represent "spin-forbidden" transitions.

help for the correct assignment of the fine structure components F_1 ($J_1 = N + 1/2$) and F_2 ($J_2 = N - 1/2$) can be achieved from the characteristic intensity pattern of the hyperfine components (F', N',) ← (F", N", J") which differs distinctively for the two fine structure components [23, 24]. For unperturbed transitions, the intensity of the hfs components increases with increasing quantum number F = J+I for the J = N + 1/2 fine-structure component but decreases for the J = N - 1/2 component (see Fig. 3). Furthermore, the wavenumbers of the line positions increase with increasing F for J=N - 1/2 but decrease for J = N + 1/2. This allows the unambiguous assignment of the quantum numbers J = N ± 1/2 and F = J + 1.

All identified rotational transitions of the measured bands in the spectral range between 15598 cm^{-1} and 15632 cm^{-1} are compiled in Table 1. The band origins ν_0 can be obtained by a least squares fit of all line positions ν in a subband with $K_a = 0$ to the formula

$$\nu = \nu_0 + B'N'(N'+1) - B''N''(N''+1). \quad (3)$$

The band origins ν_0 obtained in this way are listed in

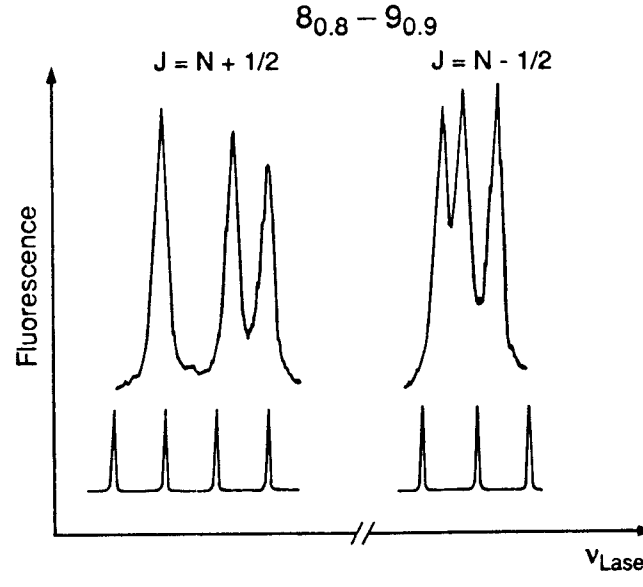

Figure 3. Hyperfine-pattern showing the characteristic intensity pattern of the hfs components
a) for the spin-component $F_1 = N + 1/2$, b) $F_2 = N - 1/2$

Table 1.

The Fortrat diagram of band No. 2 shown in Figure 4 illustrates that the spin-rotation splittings increase with N, but may vary considerably with the rotational quantum number N. For unperturbed transitions, the separation $\Delta\nu_{FS}$ of the two fine-structure components S = +1/2 and S = -1/2 should be described by the formula

$$\Delta\nu_{FS} = \Delta E' - \Delta E'' \quad \text{with } \Delta E = \varepsilon(N + 1/2). \qquad (4)$$

The spin-rotation constants in the upper levels N' may show irregular behavior (Fig. 5) and can be positive or negative depending on the strength of perturbations which may affect the two fine-structure components of the same rotational level N' differently [25]. They are listed in Table 2. This can be inspected by the appearance of "spin-forbidden" lines with $\Delta J \neq \Delta N$, which have lower intensities than the "spin-allowed" transitions with $\Delta J = \Delta N$ but can still be recognized in the spectrum [26]. These transitions are separated from the main line $\Delta N = \Delta J$ either by $\Delta\nu = \varepsilon'(N' + 1/2)$ or $\Delta\nu = \varepsilon''(N'' + 1/2)$.

The rotational constants $\bar{B}'$ averaged over all rotational lines of a band and the averaged spin-rotation constants $\bar{\varepsilon}'$ are compiled in Table 3. The fact that the constants ε' change sign for different bands can be explained by spin-orbit coupling between the upper level J' = N' ± 1/2 and high-lying levels of the $^2A_2$ state which are above the barrier to linearity and which therefore show bending vibrations where the molecule passes through the linear configuration. This gives rise to a residual effective orbital angular momentum of the electron which is not completely quenched. The shift of the term value T(N", J') de-

Table 1. Band origins and line positions of P and R lines of the four measured bands

Band 1 ν_0 = 15613.8533 cm^{-1}				Band 2: ν_0 = 15614.7976 cm^{-1}			
ν_P (cm^{-1})	ν_R (cm^{-1})	$N'_{Ka,Kc}$	S'	ν_P (cm^{-1})	ν_R (cm^{-1})	$N'_{Ka,Kc}$	S'
15613.1030	15615.6169	$1_{0,1}$	+1/2	15613.0993	15615.8016	$1_{0,1}$	+1/2
15613.2254	15615.7675	$1_{0,1}$	- 1/2	15613.2254	15615.8634	$1_{0,1}$	- 1/2
15611.0908	15616.9930	$3_{0,3}$	+1/2	15611.6168	15617.5277	$3_{0,3}$	+1/2
15610.6361	15616.5332	$3_{0,3}$	- 1/2	15611.7275	15617.6367	$3_{0,3}$	- 1/2
15610.2795	15619.5556	$5_{0,5}$	+1/2	15609.4770	15618.7558	$5_{0,5}$	+1/2
15609.1932	15618.4760	$5_{0,5}$	- 1/2	15610.2060	15619.5120	$5_{0,5}$	- 1/2
15608.8476	15621.5298	$7_{0,7}$	+1/2	15607.7306	15620.3835	$7_{0,7}$	+1/2
15607.6547	15620.3096	$7_{0,7}$	- 1/2	15608.6634	15621.3659	$7_{0,7}$	- 1/2
				15606.0833	15622.0423	$9_{0,9}$	+1/2
				15607.1400	15623.1611	$9_{0,9}$	- 1/2
				15604.0738	15623.4535	$11_{0,11}$	+1/2
Band 3: ν_0 = 15621.6861 cm^{-1}				Band 4: ν_0 = 15628.7001 cm^{-1}			
ν_P (cm^{-1})	ν_R (cm^{-1})	$N'_{Ka,Kc}$	S'	ν_P (cm^{-1})	ν_R (cm^{-1})	$N'_{Ka,Kc}$	S'
15620.2067	15622.7384	$1_{0,1}$	+1/2	15627.5018	15630.0353	$1_{0,1}$	+1/2
15620.2593	15622.7941	$1_{0,1}$	- 1/2	15627.6660	15630.2005	$1_{0,1}$	- 1/2
15618.4563	15624.3619	$3_{0,3}$	+1/2	15625.5890	15631.4986	$3_{0,3}$	+1/2
15618.5826	15624.4912	$3_{0,3}$	- 1/2	15625.1625	15631.0112	$3_{0,3}$	- 1/2
15616.6635	15625.9415	$5_{0,5}$	+1/2	15623.4537	15634.4006	$5_{0,5}$	- 1/2
15616.8590	15626.1415	$5_{0,0}$	- 1/2				
15614.7301	15627.7088	$7_{0,7}$	+1/2	15621.9557		$7_{0,7}$	+1/2

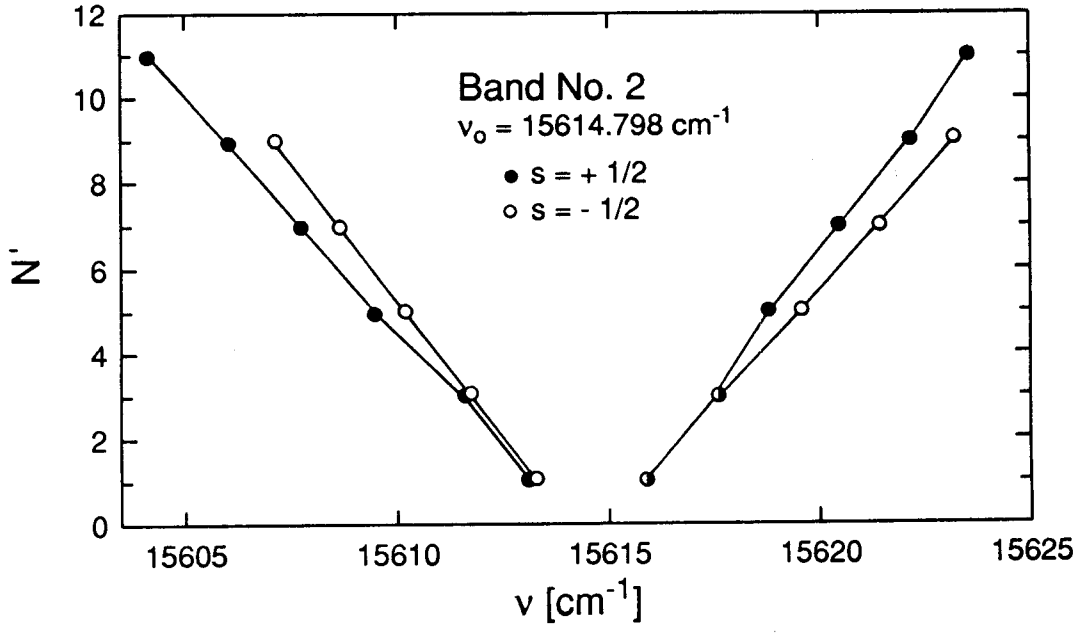

Figure 4. Fortrat diagram of the band No 2 showing the positions of the P- and R lines with their spin-rotation splitting

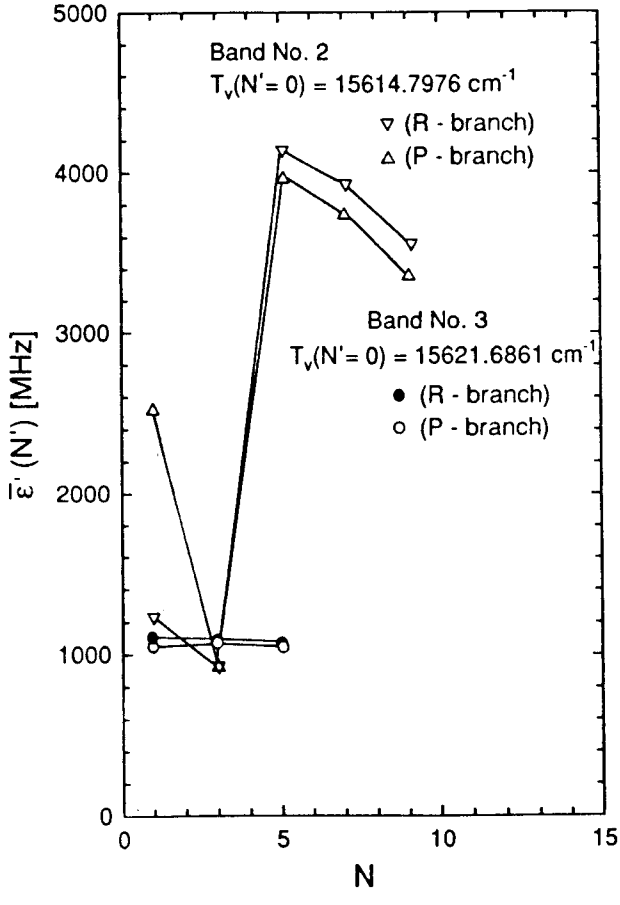

Figure 5. Spin-rotation splittings in the upper rotational levels of the four measured bands

Table 2. Spin-splittings in the upper rotational levels N'

Band	T_v[cm^{-1}]	$\bar{B}$'[cm^{-1}]	$\bar{\varepsilon}$'[cm^{-1}]
1	15613.843	0.4704	-0.1633
2	15614.798	0.4351	0.0943
3	15621.686	0.4334	0.0362
4	15628.700	0.4482	-0.0104

pends on the energy separation of the mutually perturbing levels and on the magnitude of the coupling matrix element. Its sign depends on the relative energy of the two perturbing levels. Therefore, the fine-structure levels may be pushed upwards or downwards. From the magnitude of the perturbation level shifts and the intensity of the corresponding lines the position of the perturbers can be obtained.

As has been shown in [25], the information obtained from such high resolution spectra together with optical-optical double-resonance spectroscopy, optical-radio-frequency double resonances and lifetime measurements allows one to acquire detailed information about the strength and kind of perturbations and leads to a better understanding of such a complex molecule as the excited NO_2.

The results presented in this paper contribute to the goal of gaining insight into nonlinear couplings between electronic and rovibronic degrees of freedom and to understanding the basic physics of intermolecular energy transfer in small molecules.

Table 3. Vibrational term values T_v (N' = 0), averaged rotational constants $\bar{B}$' and averaged spin-rotation constants $\bar{\varepsilon}$' of the four measured bands

Band	N'	ε'(N') [cm^{-1}]	Band	N'	ε'(N') [cm^{-1}]
	1	-0.090		1	0.063
	3	-0.131		3	0.031
1	5	-0.196	2	5	0.135
	7	-0.163		7	0.128
				9	0.115
Band	N'	ε'(N') [cm^{-1}]	Band	N'	ε'(N') [cm^{-1}]
	1	0.036		1	0.110
	3	0.037		3	0.131
3			4		
	5	0.036		3	-0.131

This may be helpful for a better understanding of such processes in large molecules where intramolecular energy transfer and conformational change in excited molecules is of great importance for chemical and biological reactions.

Acknowledgements

E. Mehdizadeh would like to thank Mahani Mathematical Research Center, Shahid Bahonar University of Kerman for partial financial support.

References

1. Hsu, D.K., Monte, D.L. and Zare, R.N. *Spectral atlas of nitrogen dioxide*. Academic Press, New York, (1978).
2. Uehara, K. and Sasada, H. *High resolution spectral atlas of nitrogen dioxide 559-597 nm*. Springer Series in Optical Sciences, Vol. 41, Springer Verlag Heidelberg, (1985).
3. Persch, G., Mehdizadeh, E., Demtröder, W., Zimmermann, Th., Köppel, H. and Cederbaum, L.S. *Ber. Bunsenges. Phys. Chem.*, **92**, 312, (1973) and *Phys. Rev. Lett.*, **61**, 3, (1988).
4. Lehmann, K.K. and Coy, St. L. *Ber. Bunsenges. Phys. Chemie*, **92**, 306, (1988).
5. Delon, A., Jost, R. and Lombardi, *M. J. Chem. Phys.*, **95**, 5701, (1991).
6. Smalley, R.E., Wharton, L. and Levy, D.H. *Ibid.*, **63**, 4977, (1975).
7. Delon, A. and Jost, R. *Ibid.*, **95**, 5686, (1991).
8. Bylicki, F., Weber, H.G., Persch, G. and Demtröder, W. *Ibid.*, **88**, 3532, (1988).
9. Jackels, C.F. and Davidson, E.R. *Ibid.*, **63**, 4672, (1975); *Ibid.*, **64**, 2908, (1976); *Ibid.*, **65**, 2941, (1976).
10. Gillispie, G.D. and Khan, A.V. *Ibid.*, **65**, 624, (1976).
11. Gillispie, G.D., Khan, A.V., Whal, A.C., Hosteny, R.P. and Kraus, M. *Ibid.*, **63**, 3425, (1975).
12. Haller, E., Köppel, H. and Cederbaum, L.S. *J. Mol. Spectrosc.*, **101**, 215, (1983) and **111**, 377, (1985).
13. Hirsch, G. and Buenker, R. J. *Can. J. Chem.*, **63**, 1542, (1985).
14. Douglas, A.E. *J. Chem. Phys.*, **45**, 1067, (1966).
15. Cheshnovsky, O. and Amirav, A. *Chem. Phys. Lett.*, **109**, 368, (1984).
16. Persch, G., Vedder, H.J. and Demtröder, W. *J. Chem. Phys.*, **105**, 471, (1988).
17. Castell, R., Demtröder, W., Fischer, A., Kullmer, R., Weickenmeier, H. and Wickert, K. *Appl. Phys.*, **B38**, 1, (1985).
18. Schweizer, W. G., Kessler, E. G., Deslattes, R.D., Layer, H.P. and Whetstone, J.R. *Appl. Opt.*, **12**, 2927, (1973).
19. Herzberg, G. *Molecular spectra and molecular structure*, Vol. 3. Van Nostrand Reinholt Company, New York, (1966).
20. Mehdizadeh, E. *J. Sci. I.R. Iran*, **1**, (3), 230, (1990).
21. Cabana, A., Lavrin, M., Lafferty, W. and Sams, R. *Can. J. Phys.*, **53**, 1902, (1975).
22. Bird, G.R., Baird, J.C., Jache, A.W., Hodgeson, J.A., Curl, R.F., Rumkle, A.C., Brandsford, J.W., Rastrup-Anderson, J. and Rosenthal, J. *J. Chem. Phys.*, **40**, 3378, (1964).
23. Persch, G., Vedder, H.J. and Demtröder, W. *J. Mol. Spectrosc.*, **123**, 356, (1987).
24. Vedder, H.J. PhD thesis, Universität Kaiserslautern, (1983).
25. Bylicki, F., Mehdizadeh, E. and Demtröder, W. *Mol. Phys.*, to be published 1993.
26. Foth, H.J. and Vedder, H.J. *J. Mol. Spectrosc.*, **102**, 148, (1983).